

Article

A Simulation on Relation between Power Distribution of Low-Frequency Field Potentials and Conducting Direction of Rhythm Generator Flowing through 3D Asymmetrical Brain Tissue

Hao Cheng ^{1,2}, Manling Ge ^{1,2}, Abdelkader Nasreddine Belkacem ³ , Xiaoxuan Fu ^{1,2,4,5}, Chong Xie ^{1,2}, Zibo Song ^{1,2}, Shenghua Chen ^{1,2,*} and Chao Chen ^{6,*}

¹ State Key Laboratory of Reliability and Intelligence of Electrical Equipment, Hebei University of Technology, Tianjin 300130, China; 202031403008@stu.hebut.edu.cn (H.C.); gemanling@hebut.edu.cn (M.G.); 201711401003@stu.hebut.edu.cn (X.F.); 201931403038@stu.hebut.edu.cn (C.X.); 201931403037@stu.hebut.edu.cn (Z.S.)

² Key Laboratory of Electromagnetic Field and Electrical Apparatus Reliability of Hebei Province, Hebei University of Technology, Tianjin 300130, China

³ Department of Computer and Network Engineering, College of Information Technology, United Arab Emirates University, Al Ain 15551, United Arab Emirates; belkacem@uaeu.ac.ae

⁴ Department of Neuroscience, Medical University of South Carolina, Charleston, SC 29425, USA

⁵ Athinoula A. Martinos Center for Biomedical Imaging, Department of Radiology, Massachusetts General Hospital/Harvard Medical School, Charlestown, MA 02115, USA

⁶ Key Laboratory of Complex System Control Theory and Application, Tianjin University of Technology, Tianjin 300384, China

* Correspondence: chenshenghua@hebut.edu.cn (S.C.); chao_chen@email.tjut.edu.cn (C.C.)



Citation: Cheng, H.; Ge, M.; Belkacem, A.N.; Fu, X.; Xie, C.; Song, Z.; Chen, S.; Chen, C. A Simulation on Relation between Power Distribution of Low-Frequency Field Potentials and Conducting Direction of Rhythm Generator Flowing through 3D Asymmetrical Brain Tissue. *Symmetry* **2021**, *13*, 900. <https://doi.org/10.3390/sym13050900>

Academic Editors:
Sebastian Ocklenburg and
Onur Güntürkün

Received: 28 April 2021
Accepted: 14 May 2021
Published: 19 May 2021

Publisher's Note: MDPI stays neutral with regard to jurisdictional claims in published maps and institutional affiliations.



Copyright: © 2021 by the authors. Licensee MDPI, Basel, Switzerland. This article is an open access article distributed under the terms and conditions of the Creative Commons Attribution (CC BY) license (<https://creativecommons.org/licenses/by/4.0/>).

Abstract: Although the power of low-frequency oscillatory field potentials (FP) has been extensively applied previously, few studies have investigated the influence of conducting direction of deep-brain rhythm generator on the power distribution of low-frequency oscillatory FPs on the head surface. To address this issue, a simulation was designed based on the principle of electroencephalogram (EEG) generation of equivalent dipole current in deep brain, where a single oscillatory dipole current represented the rhythm generator, the dipole moment for the rhythm generator's conducting direction (which was orthogonal and rotating every 30 degrees and at pointing to or parallel to the frontal lobe surface) and the (an)isotropic conduction medium for the 3D (a)symmetrical brain tissue. Both the power above average (significant power value, SP value) and its space (SP area) of low-frequency oscillatory FPs were employed to respectively evaluate the strength and the space of the influence. The computation was conducted using the finite element method (FEM) and Hilbert transform. The finding was that either the SP value or the SP area could be reduced or extended, depending on the conducting direction of deep-brain rhythm generator flowing in the (an)isotropic medium, suggesting that the 3D (a)symmetrical brain tissue could decay or strengthen the spatial spread of a rhythm generator conducting in a different direction.

Keywords: finite element method; electrical field potential; dipole moment; power; EEG

1. Introduction

Theta oscillations (4–8 Hz), which originate in deep brain cortex region, are associated with cognition and memory [1]. They can be measured not only by conducting a deep brain electroencephalogram (EEG) in vivo (local field potentials, LFPs) but also by the oscillatory field potentials (FPs) on either the frontal or temporal lobe surface via a scalp EEG [2,3]. Power fluctuation is the fundamental parameter to evaluate theta rhythms, which can reveal important information about a neural network, e.g., the extent of synchronous neurons in a local assembly. The power spectral density may be dependent on a reference

scheme at frequency bands less than 100 Hz [4,5]. In addition, power could be related to various factors such as age, long-term synaptic modification, brain structure, network state and pathology. Thus, power was generally used to investigate the scale of synchronized neurons in cognition and memory, human and animal behaviors, and even functional connectivity of rhythmic brain activity [4,6–10]. Recent evidence indicates that neural disinhibition would vary the frequency dependent LFP states such as burst, suppression and continuous. Increasing power can be observed at lower frequencies (less than 20 Hz), whereas decreasing power can be observed at higher frequencies (more than 20 Hz) in the hippocampus [11].

A consensus has not been achieved regarding the spatial spread of LFPs or FPs in the cortical medium [12–16]. The traveling theta oscillations in deep brain is an important recent observation [17], which implies that the measurement of scalp EEG rhythm at the theta frequency band considers not only some factors studied traditionally, such as the amplitude of rhythmic source current, capacitive extracellular medium, electrical conductivity and position of a rhythm generator, but also other factor such as the conducting direction of a rhythm generator. However, only some reports have investigated the latter factor [14]. Therefore, by considering the frontal lobe as an example, we attempt to map the relation between the FP power distribution on the frontal lobe surface and the conducting direction of the low-frequency rhythm generator in deep brain, based on the theory of equivalent dipole current that pertains to the generation of EEG (forward problem) [18,19].

Here, a quasi-real head surface was reconstructed from 256 T1-weighted MRI slices based on the concept of inverse engineering. The electrical conductivity of the brain tissue was described by the 3D (a)symmetrical tensor and inclusion of (an)isotropy, and the brain rhythm generator was depicted as a quasi-static dipole current in deep brain. The activity of the latter could be representative of a sine oscillation function at a low frequency (here, 6 Hz) and the moment of which could simulate the conducting direction of rhythmic source current (here, the orthogonal conducting directions, pointing to or parallel to the frontal lobe surface). Thus, a distribution of FPs evoked by the dipole current at a time point could be estimated by FEM on a quasi-real head surface by changing some simulation conditions, e.g., conductivity tensor and (an)isotropy, the position of a single dipole current and dipole moment, such as pointing to or parallel to the frontal lobe surface. During a certain time period, a simulated rhythm could be obtained based on the time series of oscillatory FPs. The instantaneous power of simulated rhythms was estimated by Hilbert transform and displayed by FPs when considering the amplitude of a single dipole current. Then, the SP area estimated by global statistics was used to study the influence of a single dipole current, such as its moment (e.g., rotating every 30°) and position (e.g., three positions inside the frontal lobe) on the SP area, by comparatively studying the anisotropic and isotropic medium with 3D asymmetrical conduction tensor and 3D symmetrical conduction tensor [20]. The flow diagram of research is shown in Figure 1.

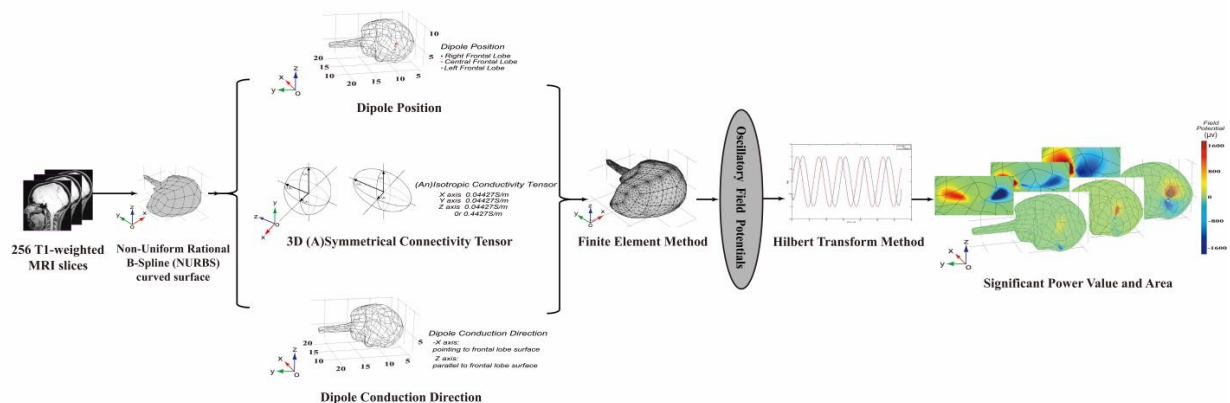


Figure 1. Flow diagram of study.

This study presents the combined effects of the low-frequency rhythm generator's conducting direction and position as well as (a)symmetrical brain tissue conductivity in mapping the FP power distribution on the head surface. Therefore, it may be helpful to further understand the generative mechanism of spontaneous low-frequency brain oscillations at the system level.

2. Methods

The power distribution was analyzed by changing some factors, i.e., the conductivity tensor and inclusion of (an)isotropy, (a)symmetrical conductivity tensor in 3D, position and conducting direction of a single dipole current on a homogeneous single-layer quasi-real head model.

2.1. Model Building

2.1.1. Reconstructed 3D Quasi-Real Head Model

Initially, a numerical model of the cortical surface was reconstructed using Simpleware (Simpleware Ltd. Corp. Exeter, UK) and then digitized using Geomagic Studio (Raindrop Ltd. Corp. Morrisville, USA), based on 256 T1-weighted MRI slices (structural MRI slices). The process required two steps. The first step was the reconstruction of a 3D quasi-real head surface model, wherein 256 sMRI images (DICOM format and 256×256 pixel matrix) were imported into scan image processing (Scan IP) module of Simpleware. In order to strip the cortical tissue from the brain tissues rapidly, the slice images were trimmed and segmented according to the gray value of the image using the interactive threshold function to segment the target area. The target area (the cerebral cortex) was removed. Surface smoothing and model configuration were employed to make the surface model more realistic, and the scalp surface model was exported in the STL format. Then, the DISCRETIZED model of head was rebuilt. The STL-format surface model was imported into Geomagic Studio. It is worth mentioning that there were still some unusable points left and the holes were missing. For the editing of unusable points, Select Outliers function and Reduce Noise function were used to remove the noise points generated by the scan moving and the noise points outside the target area. To edit the holes, they were either filled directly or a large hole diameter was dug and then filled. If the filling effect was still unsatisfactory, they were filled using the Create Point Cover function to reconstruct the area point space to repair the hole. After editing and filtering to optimize the tissue data, the holes and other drawbacks in the model were filled and repaired. The traits of the model were distinguished and extracted to build a high quality Non-Uniform Rational B-Spline (NURBS) curved surface and to generate the cortical space model (also known as reverse engineering model, R-E model). The flow chart of reconstructing the 3D quasi-real head model is shown in Figure 2.

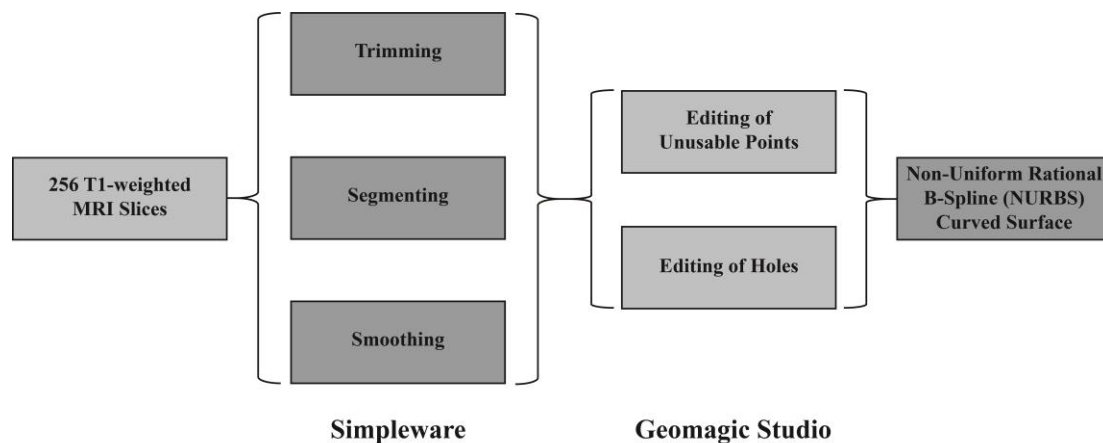


Figure 2. Flow chart of reconstructing NUBS model.

To account for the 3D elements in the finite element method, the NUBS model was layered and the key points were selected by the equal angle or equal distance method, and the nodes were connected between the layers to form a split element. The NUBS model was imported into the COMSOL Multiphysics (COMSOL Inc. Stockholm, SWE) software platform for splitting, and 35,273 elements were automatically generated under the user-controlled element/standard mode, as shown in Figure 3a. Since each element was divided into a plane on the surface of the model, the larger the curvature of the boundary of the model, the smaller the element was divided, and the more the number, the denser the unit element. Among all the elements, 3600 elements were on the frontal lobe. The isopotential lines are shown in Figure 3b, the zero-potential surface was the FP reference as shown in Figure 3c, and the alternative dipole positions are shown in Figure 3d.

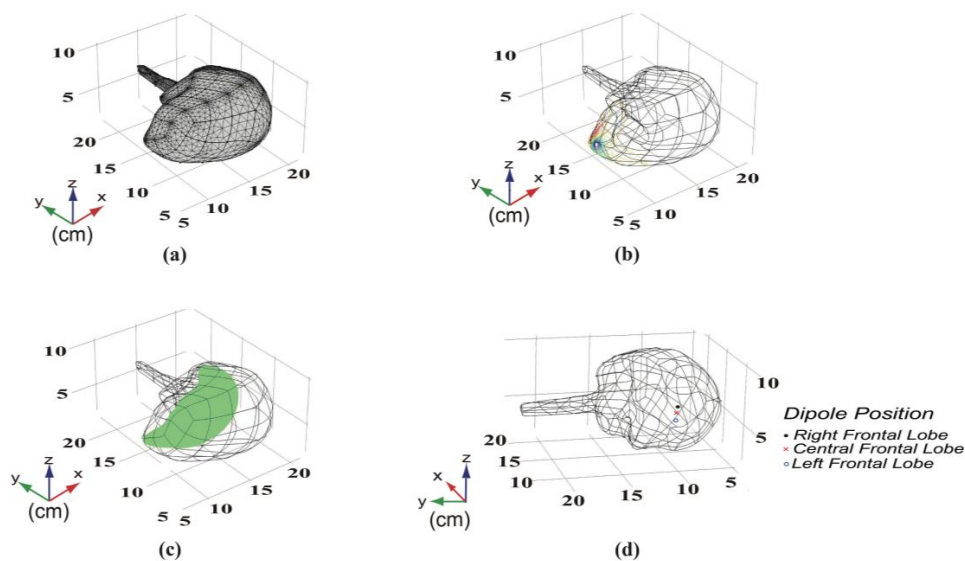


Figure 3. FP computation on the quasi-real head model surface. (a) Finite element method; (b) contour lines when the dipole current was located inside the central frontal lobe, x, y, z : 8.2, 10.9, 5.8; (c) zero-potential surface (green part); (d) schematic of alternative positions of a single dipole current (1 cm displacement along the Z axis). The dipole current amplitude was 0.1 nA.

2.1.2. Position and Conducting Direction of a Single Dipole Current

To study the influence of the position and conducting direction of a single dipole current inside the frontal lobe, the dipole direction was assumed to be the Z axis for simulating the conducting direction of dipole current parallel to the frontal lobe surface and the -X axis for the conducting direction of the dipole current pointing to the frontal lobe surface. At each dipole moment, there were three positions (denoted as right frontal lobe, central frontal lobe and left frontal lobe) with a displacement of 1 cm. Along the Z axis, the dipole position was assumed to be in the normal direction in the X-Y plane, and could be changed from the right part and middle part to the left part, the coordinates (cm) of which were (x, y, z) : 8.2, 10.9, 5.8 (right frontal lobe), (x, y, z) : 8.2, 10.9, 6.8 (central frontal lobe), and (x, y, z) : 8.2, 10.9, 7.8 (left frontal lobe), respectively, as shown in Figure 3d. In addition, along the -X axis, the dipole moment could simulate the conducting direction of a single rhythm generator pointing to the frontal lobe surface, where, the dipole position (x, y, z) : 8.2, 10.9, 6.8 was localized inside the central frontal lobe. Thus, the near frontal lobe (x, y, z) : 7.2, 10.9, 6.8 represented carrying the dipole current near to the lobe surface, whereas the far frontal lobe (x, y, z) : 9.2, 10.9, 6.8 represented carrying the dipole current far away from the lobe surface.

2.1.3. Symmetrical Conductivity and Asymmetrical Conductivity

The mean electrical conductivity was considered in this study [21]. Ideally, the conducting medium must be isotropic with the 3D symmetrical conductivity tensor of $\sigma_x = \sigma_y = \sigma_z = 0.14$ S/m. However, the conducting medium was anisotropic in a real brain with the 3D asymmetrical conductivity tensor of $\sigma_x = \sigma_y = 0.04427$ S/m, $\sigma_z = 0.4427$ S/m, i.e., $\sigma_x : \sigma_z = 1 : 10$. Here, the influence of anisotropic conductivity was compared with that of isotropic conductivity, where the influence of a 3D asymmetrical conductivity tensor was comparatively studied with that of a 3D symmetrical conductivity tensor. The isotropic conductivity medium tensor is shown in Formula (1), and the anisotropic conductivity medium tensor is shown in Formula (2).

$$\sigma = \begin{bmatrix} \sigma_x & \sigma_{xy} & \sigma_{xz} \\ \sigma_{yx} & \sigma_y & \sigma_{yz} \\ \sigma_{zx} & \sigma_{zy} & \sigma_z \end{bmatrix} = \begin{bmatrix} 0.14 & 0 & 0 \\ 0 & 0.14 & 0 \\ 0 & 0 & 0.14 \end{bmatrix} \quad (1)$$

$$\sigma = \begin{bmatrix} \sigma_x & \sigma_{xy} & \sigma_{xz} \\ \sigma_{yx} & \sigma_y & \sigma_{yz} \\ \sigma_{zx} & \sigma_{zy} & \sigma_z \end{bmatrix} = \begin{bmatrix} 0.04427 & 0 & 0 \\ 0 & 0.04427 & 0 \\ 0 & 0 & 0.4427 \end{bmatrix} \quad (2)$$

2.2. Calculation Derivation

2.2.1. FP Derivations of Low-Frequency Simulated Rhythms

A generalized expression of the forward problem, i.e., the theory of the equivalent dipole current with respect to the generation of EEG, could be helpful to facilitate mapping [18,19]. Given the position and moment of a static equivalent dipole current generator and the geometry and electrical conductivity (σ) profile of the volume conductor (Ω , i.e., model of the head), the electrical FPs (ψ) can be considered as EEG and could be expressed by Poisson's equation and the Neumann boundary condition. This is a very authoritative method since it was released in 1978 and is still in use today [18] on the head surface (S).

$$\nabla \cdot (\sigma \cdot \nabla \psi) = - \sum_{\Omega} J_s \quad (\text{in } \Omega) \quad (3)$$

$$\sigma(\nabla \psi) \cdot n = 0 \quad (\text{on } S) \quad (4)$$

Here, n is the normal direction of the boundary and J_s is the electric current density of a conductor.

The rhythms were simulated by oscillatory electrical FPs on a 3D quasi-real head surface model (single-layer homogeneous medium), which was obtained via FEM using COMSOL Multiphysics. The activity of the dipole current was a sine function with an amplitude of 0.1 nA, a frequency of 6 Hz and an initial phase of 0 radian when considering a time window of 1 s. The dipole current can be considered as the rhythm generator and the electrical field evoked by a single dipole current was quasi-static. Additionally, the electrical FP could be calculated by FEM at each time point at each generated element. A time course of 1 s with respect to the dipole current was split into 128 equal time points. The oscillating electrical FP was considered as the simulated rhythm on each element during this 1 s period.

2.2.2. FP Power Derivations of Low-Frequency Simulated Rhythms

The low-frequency oscillatory FP is a continuous signal, which is denoted as $FP(t)$. $FP(t)$ was Hilbert transformed (hilbert, MATLAB) to get $\widetilde{FP}(t)$ and can be expressed as follows.

$$\widetilde{FP}(t) = \frac{1}{\pi} p.v. \int_{-\infty}^{+\infty} \frac{A(\tau) e^{j\phi_{FP}(\tau)}}{t - \tau} d\tau \quad (5)$$

Here, $A(\tau)$ is the instantaneous amplitude of $FP(t)$, $\phi_{FP}(\tau)$ is the instantaneous phase of $FP(t)$, and $p.v.$ is the Cauchy principal value.

For a continuous signal, its instantaneous power value is equal to the square of the signal modulus after Hilbert transformation of the signal. This is to say the instantaneous power was a sum of the square of the real part plus the square of the imaginary part of the oscillatory FPs., The power was then averaged over time.

2.2.3. Value and Area of Significant Power

Power values greater than the mean power (significant power, denoted as, i.e., SP), were a concern to study the influence of the position strength and conducting direction of a rhythm generator on the significant power distribution. In addition, the SP area (%) was defined as the ratio of the number of elements with an SP value to the total number of elements needed to study the influence space. Moreover, the SP area was displayed by a spatial sum of a warm color tone plus a cold color tone on a standard colormap of FPs corresponding to a rhythm generator at an amplitude of 0.1 nA. According to the partial volume effect [22], the larger the SP area, the smaller the significant FP power value. This suggests that a greater space influence will mean a weaker influence of strength, and vice versa.

The subsequent statistical significance of the FP power was determined between anisotropic medium and isotropic medium, where the dipole moment was parallel to and pointing to the frontal lobe surface and the adjacent displacement distance of a single dipole current. The student's unpaired t-test was used to determine the statistical significance.

2.3. Validation Influence of Conducting Direction

The influence of the conducting direction of the rhythm generator on the SP area was validated by rotating the conduction direction of a single dipole current at every 30° of the rotation under two conditions, i.e., pointing to or parallel to the lobe surface, when the dipole current was at the central inside frontal lobe. The dipole moment was rotated (i) departing from the -X axis via the Y axis and arriving at the opposite site (X axis); (ii) departing from the Z axis via the Y axis and arriving at the opposite site (-Z axis).

3. Results

There were 3600 elements present from left to right on the frontal lobe surface; thus, the power values of these elements were considered during the analysis.

3.1. Distribution of Significant Power at Dipole Moment Pointing to Frontal Lobe Surface

The distribution of FP power when a dipole current was flowing directly to the frontal surface (dipole moment at the -X axis) is shown in Figure 4. From the horizontal perspective, i.e., isotropic medium (left panel) compared to anisotropic medium (right panel), the SP area was greatly reduced in the anisotropic medium relative to that in the isotropic medium ($p < 0.001$), suggesting that the 3D asymmetrical conductivity tensor of brain tissue could strengthen an ongoing dipole current in deep brain, thereby resulting in the SP area to reduce on the frontal lobe surface. From the vertical perspective, because of the dipole current position, the partial volume effect could be observable, i.e., the smaller the SP area, the greater the SP values, suggesting the opposite effects indicated by the SP area and the SP value. At a distance of 1 cm, the maximum power values differed by more than a factor of two, as indicated by the maximum value using the color bars.

3.2. Distribution of Significant Power at Dipole Moment Parallel to Frontal Lobe Surface

The FP power distribution when a dipole current was flowing parallel to the frontal lobe surface (dipole moment at the Z axis) is shown in Figure 5. From the horizontal perspective, the SP area considerably increased in the anisotropic medium (right panel) compared to that in the isotropic medium (left panel) ($p < 0.001$), suggesting that the 3D asymmetrical conductivity tensor of brain tissue could weaken an ongoing dipole current in deep brain. This would result in the SP area increasing on the frontal lobe surface, which is the reverse of the effect shown in Figure 4. However, from the vertical perspective,

the partial volume effect is similar to that shown in Figure 4, i.e., the smaller the SP area, the greater the SP values.

3.3. Validation of Influence of Dipole Moment on Area of Significant Power

In Figure 6, the SP area was shown by rotating the dipole moment after every 30° in two directions, pointing to and parallel to the frontal surface. When considering the condition of the dipole moment flowing along the frontal lobe, an increased SP area was observed on the frontal lobe surface in the anisotropic medium relative to the isotropic medium, implying that the 3D asymmetrical conductivity of brain tissue could decay the ongoing dipole current. In reverse, a decreased SP area was observed when considering the condition of the dipole moment flowing directly to the frontal lobe. This implies that the 3D asymmetrical conductivity of brain tissue could enhance the ongoing dipole current, except under some specific conditions, such as the Y axis (parallel to the frontal lobe surface) and X axis (pointing to deep brain), as shown in Figure 6a.

Taken together, as long as the dipole moment is flowing along the frontal lobe, the 3D asymmetrical conductivity of brain tissue could weaken the ongoing dipole current, leading to an increase in SP area which was observed on the frontal lobe surface in the anisotropic medium.

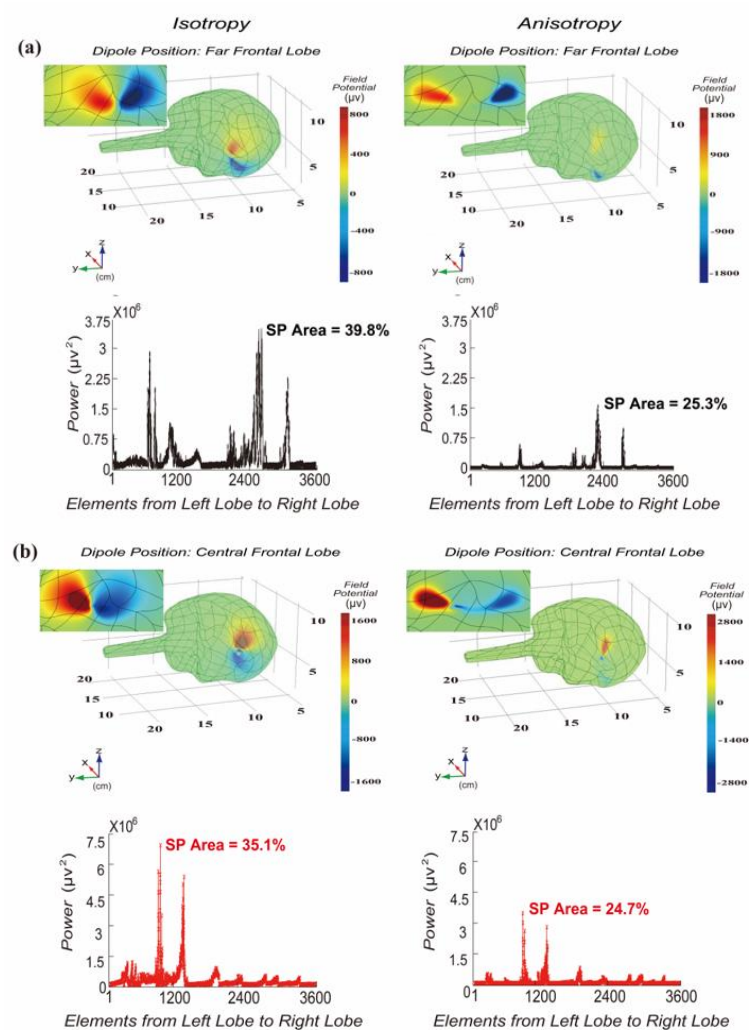


Figure 4. Cont.

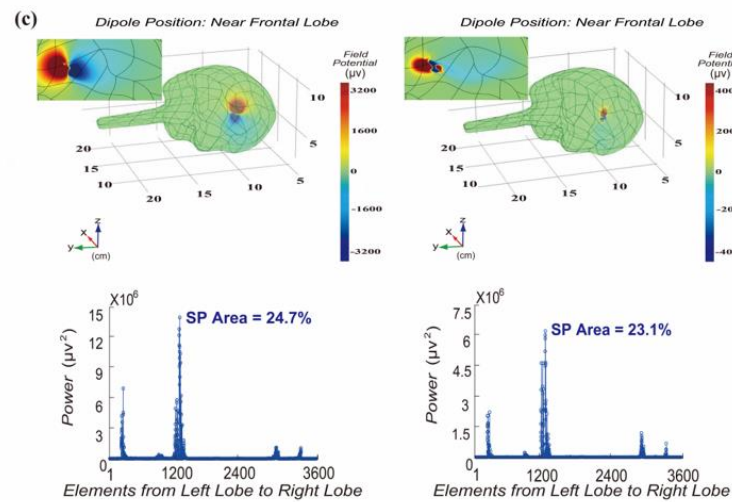


Figure 4. Influence of dipole current position on distribution of FP power, when a dipole current is flowing directly to the frontal lobe surface and is conducted in an isotropic medium (left panel) or an anisotropic medium (right panel). (a) Located far from the frontal lobe; (b) located inside the central frontal lobe; (c) located near to the frontal lobe. Each sub-picture contains an FP distribution figure with partially enlarged picture.

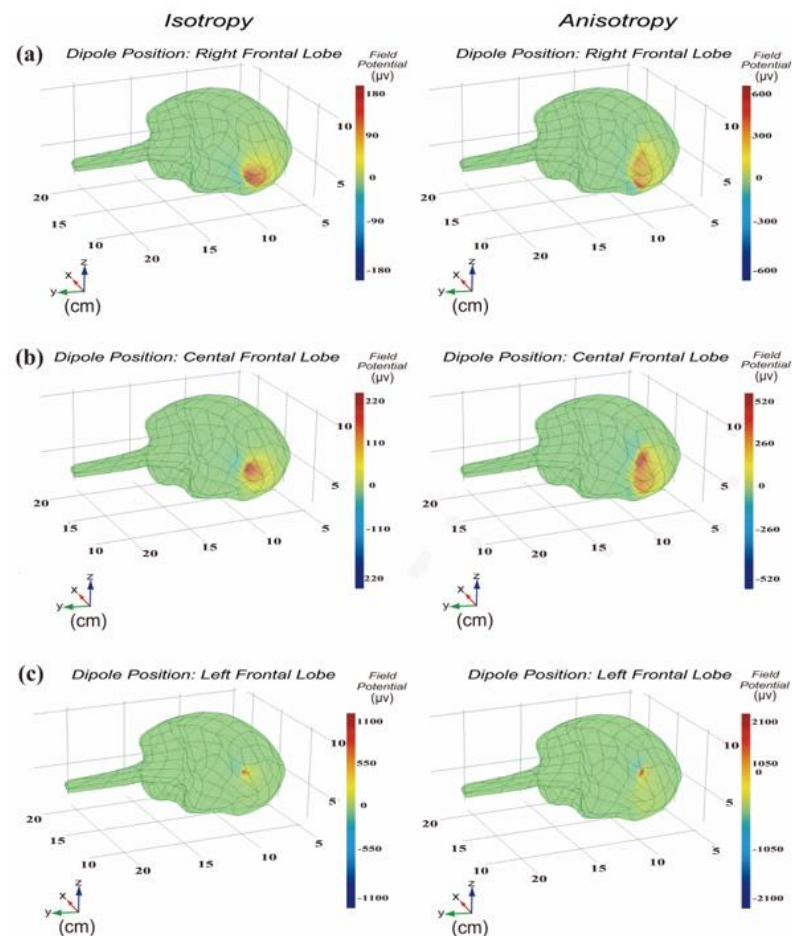


Figure 5. Influence of dipole current's position on distribution of FP power, when a dipole current is flowing parallel to the frontal lobe surface and is conducted in an isotropic medium (left panel) or an anisotropic medium (right panel). (a) Located inside the right frontal lobe; (b) located inside the central frontal lobe; (c) located inside the left frontal lobe.

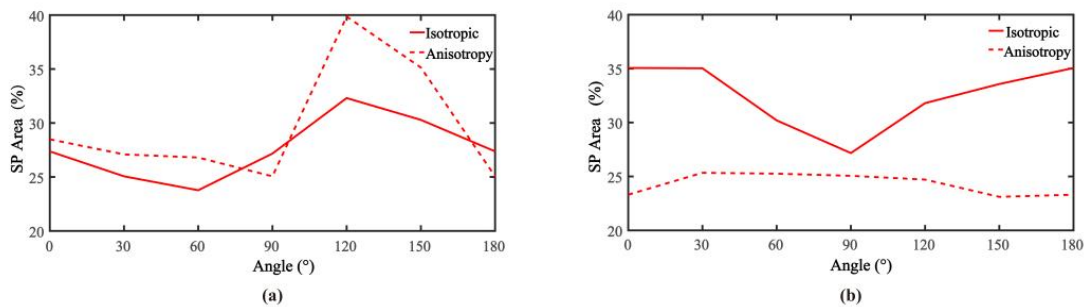


Figure 6. Influence of dipole moment on the SP area. (a) Direct to the frontal lobe surface, departing from -X axis and arriving at backward via Y axis (90 degree); (b) along the frontal lobe surface, departing from Z axis and arriving at backward via Y axis (90 degree).

4. Discussion

4.1. Power

As shown in Figures 4 and 5, the distribution of significant FP power could be reversed in the (an)isotropic medium in the orthogonal directions of the rhythm generator in deep brain. This implies a joint consequence of the conducting direction of rhythmic source current and the complex conductivity of brain tissue. This consequence can be further explained by the solution of FPs on a spherical surface in the forward problem, i.e., the FPs evoked by the dipole current were inversely proportional to the square of the distance to the rhythm generator. The closer the distance between an element and the rhythm generator, the stronger the FP rhythms and the greater the significant FP power values [18,23].

The distance between the dipole source current and the lobe surface was approximately equal when the dipole current flowed along the frontal lobe; thus, distance was a minor factor. However, the disturbance in anisotropic conductivity was a significant factor that resulted in more SP area in the 3D electrical field relative to the balance in isotropic conductivity. Consequently, the SP area in the anisotropic medium was greater than that in the isotropic medium, as shown in Figures 4 and 5.

Moreover, in Figure 6a, in some specific conditions such as the Y axis (parallel to the frontal lobe surface) the effect of anisotropy of brain tissue isn't an exception, because its effect is convergent to that as shown in Figure 6b.

In previously conducted neural measurement studies, power reflected the strength of brain rhythms, which were related to many factors such as brain regions, scale of synchronous neurons, brain function, pathology and physiology [2,7,10,24]. Our theoretical work further suggests that FP power was dependent on the combined factors that were difficult to measure at a system level, including the position of a rhythm generator, brain tissue conductivity and even the conducting direction of a rhythm generator in deep brain.

4.2. Anisotropy

A formation of grey matter and white matter is a basis of the conductivity of brain tissue. In the human brain, anisotropy is related to the fiber architecture of cortex and laminae and the gross anatomical regions related to cortical gyri and local curvature. The anisotropy is a consequence of a difference in conductivity of different tissues and matter types in the brain. Anisotropy could be measured using various technologies such as echo planar imaging and diffusion tensor imaging. Previous work has shown anisotropy could be associated with brain physiology and pathology [25,26], with a 10-fold relationship at the Z axis tensor where only one variable factor was required to produce an anisotropy. Our work chose this setting by which the influence of asymmetric conductivity on the propagation of deep-brain rhythm sources could be found significantly compared to symmetric conductivity. In a real system, either the anisotropy or the propagation direction of a deep-brain rhythm generator could be far more complicated than this anisotropic setting and the representation of conducting direction in this study. There is currently no

clear conclusion on the parameters that would model the real brain anisotropy and the propagation pathway of a low-frequency brain rhythm generator. From the perspective of overall brain physiology, the anisotropic model is more realistic, and isotropic model is ideal. However, by comparing the conduction of isotropic media, it can also provide a reference for the conduction effect of isotropic local brain tissues.

5. Conclusions

On the frontal lobe surface, the space distribution of significant EEG rhythm power (SP area) in a low-frequency frequency band was investigated via simulation. The SP area was considerably affected by many factors. The anisotropy of brain tissue with 3D asymmetrical conduction tensor could limit or enlarge the available recording area of significant power, depending on the conducting direction of the rhythm generator in deep brain. Considering the partial volume effect, the narrower the SP area, the greater the power values. This result implies that the accurate and cautious placement of EEG electrodes is very important during measurement, and that traditional analysis on mean power must be conducted under very strict conditions such as potential localization and possible spread pathway of the rhythm generator in deep brain. Therefore, this study may be helpful to researchers and practitioners involved with the measurement and analysis of spontaneous low-frequency EEG rhythms at a system level.

To the best of our knowledge, the simulation described in this study is the first to report the 3D asymmetrical conduction characteristic of anisotropic conductivity tensor. Future investigations should focus on linking the shapes of gray and white matter, anisotropic tissue and other related factors to study their influence on low-frequency rhythms on the head surface.

Author Contributions: Conceptualization, H.C. and M.G.; methodology, H.C., M.G. and S.C.; software, H.C. and X.F.; validation, H.C. and C.X.; formal analysis, H.C. and Z.S.; resources, M.G. and S.C.; data curation, H.C. and X.F.; writing—original draft preparation, H.C. and M.G.; writing—review and editing, H.C., M.G., A.N.B. and C.C.; visualization, H.C. and X.F.; supervision, M.G., S.C. and C.C.; project administration, H.C. and M.G.; funding acquisition, M.G., S.C. and C.C. All authors have read and agreed to the published version of the manuscript.

Funding: The work is partly financially supported by Grants sponsored by Hebei Province (E2019202019/ZD2021025). Fu Xiaoxuan is supported by Medical University of South Carolina as a research assistant (Program Number: P-1-00715) and Chen Chao is supported by in part by National Natural Science Foundation of China (61806146) and National Key Research & Development Program of China (2018YFC1314500).

Institutional Review Board Statement: The study was conducted according to the guidelines of the Declaration of Helsinki, and approved by the Biomedical Ethics Committee of Hebei University of Technology (protocol code: HEBUThMEC2021015 and date of approval: January 2021).

Informed Consent Statement: Informed consent was obtained from all subjects involved in the study.

Data Availability Statement: Not applicable.

Conflicts of Interest: The authors declare no conflict of interest.

References

1. McDonnell, J.; Murray, N.P.; Ahn, S.; Clemens, S.; Everhart, E.; Mizelle, J.C. Examination and Comparison of Theta Band Connectivity in Left- and Right-Hand Dominant Individuals throughout a Motor Skill Acquisition. *Symmetry* **2021**, *13*, 728. [[CrossRef](#)]
2. Buzsáki, G. *Rhythms of the Brain*; Oxford University Press: Oxford, UK, 2009.
3. Herweg, N.A.; Solomon, E.A.; Kahana, M.J. Theta Oscillations in Human Memory. *Trends Cogn. Sci.* **2020**, *24*, 208–277. [[CrossRef](#)]
4. Fu, X.; Wang, Y.; Ge, M.; Wang, D.; Gao, R.; Wang, L.; Guo, J.; Liu, H. Negative Effects of Interictal Spikes on Theta Rhythm in Human Temporal Lobe Epilepsy. *Epilepsy Behav.* **2018**, *87*, 207–212. [[CrossRef](#)]
5. Shirhatti, V.; Borthakur, A.; Ray, S. Effect of Reference Scheme on Power and Phase of the Local Field Potential. *Neural Comput.* **2016**, *28*, 882–913. [[CrossRef](#)]

6. Alarcon, G.; Binnie, C.D.; Elwes, R.D.C.; Polkey, C.E. Power Spectrum and Intracranial EEG Patterns at Seizure Onset in Partial Epilepsy. *Electroencephalogr. Clin. Neurophysiol.* **1995**, *94*, 326–337. [[CrossRef](#)]
7. Chauvière, L.; Raftafi, N.; Thinus-Blanc, C.; Bartolomei, F.; Esclapez, M.; Bernard, C. Early Deficits in Spatial Memory and Theta Rhythm in Experimental Temporal Lobe Epilepsy. *J. Neurosci.* **2009**, *29*, 5402–5410. [[CrossRef](#)]
8. Ge, M.; Wang, D.; Dong, G.; Guo, B.; Gao, R.; Sun, W.; Zhang, J.; Liu, H. Transient Impact of Spike on Theta Rhythm in Temporal Lobe Epilepsy. *Exp. Neurol.* **2013**, *250*, 136–142. [[CrossRef](#)] [[PubMed](#)]
9. Lindén, H.; Pettersen, K.H.; Einevoll, G.T. Intrinsic Dendritic Filtering Gives Low-pass Power Spectra of Local Field Potentials. *J. Comput. Neuroence* **2010**, *29*, 423–444. [[CrossRef](#)] [[PubMed](#)]
10. Winson, J. Loss of Hippocampal Theta Rhythm Results in Spatial Memory Deficit in the Rat. *Science* **1978**, *201*, 160–163. [[CrossRef](#)]
11. Miriam, G.; Markus, B.; Tobias, B. Frequency- and State-dependent Effects of Hippocampal Neural Disinhibition on Hippocampal Local Field Potential Oscillations in Anesthetized Rats. *Hippocampus* **2020**, *30*, 1021–1043.
12. Agrita, D.; Supratim, R. Spatial Spread of Local Field Potential is Band-pass in the Primary Visual Cortex. *J. Neurophysiol.* **2016**, *116*, 1986–1999.
13. Bédard, C.; Rodrigues, S.; Roy, N.; Contreras, D.; Destexhe, A. Evidence for Frequency-dependent Extracellular Impedance from the Transfer Function between Extracellular and Intracellular Potentials. *J. Comput. Neurosci.* **2010**, *29*, 389–403. [[CrossRef](#)]
14. Ge, M.; Fu, X.; Zhang, J.; Chen, S.; Chen, Y.; Gao, R.; Zhang, H. The Influences of Tissue Anisotropy and Source Activity on Power and Phase Stability of Low-frequency EEG Rhythms: A Mathematical Observation of the Forward Problem Model. *Biomed. Phys. Eng. Express* **2016**, *2*. [[CrossRef](#)]
15. Łęski, S.; Lindén, H.; Tetzlaff, T.; Pettersen, K.H.; Einevoll, G.T. Frequency Dependence of Signal Power and Spatial Reach of the Local Field Potential. *PLOS Comput. Biol.* **2013**, *9*, e1003137. [[CrossRef](#)]
16. Logothetis, N.K.; Kayser, C.; Oeltermann, A. In vivo Measurement of Cortical Impedance Spectrum in Monkeys: Implications for Signal Propagation. *Neuron* **2007**, *55*, 809–823. [[CrossRef](#)]
17. Lubenov, E.V.; Siapas, A.G. Hippocampal Theta Oscillations are Travelling Waves. *Nature* **2009**, *459*, 534–539. [[CrossRef](#)]
18. Brody, D.A.; Terry, F.H.; Ideker, R.E. Eccentric Dipole in a Spherical Medium: Generalized Expression for Surface Potentials. *IEEE Trans. Bio. Med. Eng.* **1973**, *20*, 141–143. [[CrossRef](#)] [[PubMed](#)]
19. Torres, F. Electroencephalography: Basic Principles, Clinical Applications and Related Fields. *Arch. Neurol.* **1983**, *40*, 191–192. [[CrossRef](#)]
20. Vecchio, A.; De Pascalis, V. EEG Resting Asymmetries and Frequency Oscillations in Approach/Avoidance Personality Traits: A Systematic Review. *Symmetry* **2020**, *12*, 1712. [[CrossRef](#)]
21. Nicholson, P.W. Specific Impedance of Cerebral White Matter. *Exp. Neurol.* **1965**, *13*, 386–401. [[CrossRef](#)]
22. Soret, M.; Bacharach, S.L.; Buvat, I. Partial-volume Effect in PET Tumor Imaging. *J. Nucl. Med.* **2007**, *48*, 932–945. [[CrossRef](#)]
23. De Munck, J.C.; Wolters, C.; Clerc, M. EEG and MEG: Forward Modeling. In *Handbook of Neural Activity Measurement*; Brette, R., Destexhe, A., Eds.; Cambridge University Press: Cambridge, UK, 2012; pp. 192–256.
24. Ding, N.; Simon, J.Z. Power and Phase Properties of Oscillatory Neural Responses in the Presence of Background Activity. *J. Comput. Neuroence* **2013**, *34*, 337–343. [[CrossRef](#)]
25. Satzer, D.; Lanctin, D.; Eberly, L.E.; Abosch, A. Variation in Deep Brain Stimulation Electrode Impedance over Years Following Electrode Implantation. *Stereotact. Funct. Neurosurg.* **2014**, *92*, 94–102. [[CrossRef](#)] [[PubMed](#)]
26. Wolters, C.H.; Anwander, A.; Tricoche, X.; Weinstein, D.; Koch, M.A.; Macleod, R.S. Influence of Tissue Conductivity Anisotropy on EEG/MEG Field and Return Current Computation in a Realistic Head Model: A Simulation and Visualization Study Using High-resolution Finite Element Modeling. *NeuroImage* **2006**, *30*, 813–826. [[CrossRef](#)]